

Vorticity and geopotential height extreme values in ERA-Interim data during boreal winters

R. Blender,^{a*} C. C. Raible^b and C. L. E. Franzke^a

^aMeteorological Institute and Center for Earth System Research and Sustainability (CEN), University of Hamburg, Germany

^bClimate and Environmental Physics and the Oeschger Centre for Climate Change Research, University of Bern, Switzerland

*Correspondence to: R. Blender, Meteorologisches Institut, Universität Hamburg, Grindelberg 5, D-20144 Hamburg, Germany.
E-mail: richard.blender@uni-hamburg.de

The properties and dependences of lower tropospheric geopotential height (GPH) and relative vorticity extreme values are investigated in high spatial resolution ERA-Interim reanalysis data during the boreal winters from 1980–2014. A peak-over-threshold (POT) analysis is applied to determine the local generalized Pareto distribution (GPD) parameters with a 90th percentile threshold. In Northern Hemispheric storm tracks, the scale parameter decreases along the storm track axis for vorticity, whereas it increases for GPH. The shape parameters are weakly negative for both fields in the northern midlatitudes and over land, suggesting upper bounds for the extremes. The association of GPD parameters with the large-scale flow is assessed using monthly mean indices for the North Atlantic Oscillation (NAO), Pacific–North American (PNA) pattern and El Niño Southern Oscillation (Nino3.4 index) as covariates. While the GPH parameters are related to the covariates in the regions associated with the covariate loadings, the vorticity parameters are weakly related to all covariates. It is noteworthy that the NAO dominates all covariates in the central tropical Pacific. The probability for concurrent extreme events of vorticity and GPH is highest in storm tracks with values of about 0.3–0.5.

Key Words: vorticity; geopotential height; extremes; covariates; extreme dependence; predictability

Received 21 June 2016; Revised 11 October 2016; Accepted 17 October 2016; Published online in Wiley Online Library 30 November 2016

1. Introduction

Extreme weather events are an important part of the general circulation and can cause significant economic damages. For instance, European wind storms can cause damages of about 2 billion euros each and are listed as one of the major natural hazard threats to Europe (Malmquist, 1999; MunichRe, 2010; MunichRe, 2015). The attribution and estimation of losses due to wind storms is thus an active area of research (Klawa and Ulbrich, 2003; Schwierz *et al.*, 2010; Held *et al.*, 2013; Welker and Martius, 2014).

The severity of storms depends on the large-scale circulation (Raible, 2007) and atmospheric regime states (Franzke *et al.*, 2011; Franzke, 2013). We analyze the extremes as threshold exceedances (Coles, 2001; Raible, 2007) and fit the generalized Pareto distribution (GPD; Coles, 2001; Franzke, 2013). Analyzing North Atlantic surface wind speeds, Franzke (2013) found that the shape parameter of the GPD distribution is negative, which suggests the existence of an upper bound of wind-speed extremes (Coles, 2001). These results are consistent with theoretical considerations about tail decay for climate variables by Majda *et al.* (2009).

Extreme wind speeds in the North Atlantic region are associated with strong midlatitude cyclones (e.g. Leckebusch and Ulbrich, 2004). Although midlatitude cyclones are well-known

phenomena, there is no general agreement on a definition based on a single field (Raible *et al.*, 2008; Neu *et al.*, 2013). Midlatitude cyclones are determined either by geopotential height (GPH; or pressure) minima or relative vorticity maxima (in the following we will use vorticity for short; see e.g. Hodges, 1994; Blender *et al.*, 1997; Simmonds and Keay, 2000), or a combination of both (Murray and Simmonds, 1991a, 1991b; Koenig *et al.*, 1993). The methods have recently been intercompared for reanalysis data (Neu *et al.*, 2013) and scenario simulations of future global warming (Ulbrich *et al.*, 2013). Whether cyclones are detected using either GPH or vorticity depends, amongst other things, on the resolution of the data. As both fields are related in a balanced flow, it is expected that there is an agreement in the detection of large vorticities to some degree. The variables have specific advantages and disadvantages. For example, since vorticity in the lower troposphere includes fronts in high-resolution data, a clear identification of vortices is hampered. In this case, it is helpful to consider a lower resolution (Hodges, 1994). On the other hand, GPH minima are displaced and even hidden in the mean flow. Tracking schemes combining GPH minima and vorticity maxima, e.g. in the Melbourne University tracking algorithm, reduce interruptions caused by weak cyclones (see the analysis of Mediterranean cyclones in Flocas *et al.* (2010) and references therein).

Further, extreme cyclones are linked to the large-scale circulation. In the North Atlantic, the dependence of extreme cyclones on the North Atlantic Oscillation (NAO) discussed in Sienz *et al.* (2010) resembles the findings of Pinto *et al.* (2008), who focused on the 10% most intense cyclones. The frequency of deep cyclones and their relationship to the NAO and Pacific–North America pattern (PNA) has been studied in National Centers for Environmental Prediction (NCEP)/National Center for Atmospheric Research (NCAR) reanalysis data by Gulev *et al.* (2001). According to their study, the NAO controls the latitudinal shift in the North Atlantic, while the PNA is responsible for variability of the frequency of deep cyclones in the Eastern Pacific.

Given these discrepancies and the dependence of extremes on the large-scale circulation, the aim of this study is to determine properties and relationships between extremes of low-level relative vorticity and GPH, focusing on the two Northern Hemispheric storm track areas and boreal winters. Thereby the analysis is threefold.

- (i) Extreme values of vorticity and GPH are diagnosed by a peak-over-threshold (POT) analysis (Coles, 2001).
- (ii) The relationship between the GPD parameters and large-scale flow indices is investigated using covariates. Thereby, we use monthly mean indices for NAO, PNA and Nino3.4. The Nino3.4 index is included because of the high seasonal predictability by atmosphere–ocean models.
- (iii) The dependence of concurrent vorticity and GPH extremes is assessed using two measures suggested by Coles *et al.* (1999) to exclude the diagnostics of spurious dependences in independent data. The dependence of concurrent vorticity and GPH extremes sheds light on the appropriate definition of lows and is relevant for detection methods.

This article is organized as follows. The data are described in section 2 and the extreme value diagnostics in terms of the GPD in section 3. The results are presented in section 4 and summarized in section 5.

2. Data

The data analyzed in this study are 850 hPa vorticity and 1000 hPa GPH from the ERA-Interim reanalysis (Dee *et al.*, 2011). The data have a spatial resolution of 0.75° covering the period 1 December 1979–28 February 2014. The analysis is based on boreal winter (December–February, DJF). Thus, the first winter consists of January–February data only; the last winter is DJF in 2013/2014. To concentrate on the synoptic variability, we use daily data at 0000 UTC (Coordinated Universal Time). The time series are not processed, e.g. by declustering, since we are also interested in the dependence of concurrent vorticity and GPH extremes (see aim (iii) in section 1). As large-scale covariates, we use monthly means of the indices for the NAO, PNA and Nino3.4 from the Climate Prediction Center of the National Oceanic and Atmospheric Administration (NOAA).

3. Extreme value statistics and covariates

Extremes are analyzed by the POT approach (Coles, 2001) with a threshold u given by the 90th percentile determined separately for each grid point. Extreme minima in the data are analyzed as (positive) extremes of the negative data (by multiplying them by -1). The exceedences $x - u$ of the data x are asymptotically distributed according to the GPD. The GPD is a family of distributions for the argument $z = (x - u)/\sigma$ with a scale parameter σ and a shape parameter ξ , which determine the decay and the support of the distribution:

$$f(z, \xi) = \begin{cases} (\xi z + 1)^{-(1+\xi)/\xi} & \xi \neq 0, \\ \exp(-z) & \xi = 0. \end{cases} \quad (1)$$

For positive values, $\xi \geq 0$ (the Pareto or Fréchet limit), the support of the probability density is given by positive arguments, $z \geq 0$. For negative shape parameters, $\xi < 0$ (the reversed Weibull limit), the support has an upper bound, $0 \leq z \leq -1/\xi$; beyond this value, the density vanishes. Negative shape parameters can be found erroneously, as a small sample can yield a bias in the parameter estimation. On the other hand, negative shape parameters can hint at a physical upper bound in a variable. For a discussion of the role and properties of the shape parameter in dynamical systems theory, see Lucarini *et al.* (2014).

Covariates are linear predictors for parameters of extreme value distributions (see Coles, 2001 and the application to North Atlantic cyclones and the NAO index by Sienz *et al.*, 2010). To obtain relevant results, the significance of a predictor has to be determined by a comparison with the so-called stationary model. This stationary model is defined by fitting without any covariate.

The parameters in the GPD are modelled as functions of an external time-dependent parameter $Y(t)$, the covariate. In this investigation, the scale parameter is fitted with a linear model:

$$\sigma = \sigma_0 + \sigma_1 Y, \quad (2)$$

with a constant term σ_0 and sensitivity σ_1 . The formula for the shape parameter is analogous. Covariates are widely used as predictors for the modelling of extremes assuming causal relationships (Coles, 2001).

By using covariates, an analysis is possible in non-stationary conditions. If the impact of a linear climatological trend is assessed, time can be used as a covariate $Y(t) = t$. The covariate analysis adds a predictive aspect in extreme value statistics (EVS). The dependence of the extremal properties on large-scale and slowly varying covariates reveals mechanisms and allows a prediction (Franzke, 2013).

Note that the dependence pertains only to the scale and the shape parameters, whereas the threshold u remains constant in the GPD fit. The change of intensity is not accessible. This differs from a block maximum analysis with a generalized extreme value distribution fit, which includes an additional location parameter. Thus, the dependence of the intensity on covariates is accessible (for an application in hydrology, see Towler *et al.*, 2010).

A main result is the significance of the covariate model (the values of the coefficients σ_0 and σ_1 are not considered here). This is assessed by the deviance statistic (Coles, 2001):

$$D = 2(L_1 - L_0), \quad (3)$$

determined by the log-likelihoods L_0 of the stationary model and L_1 for the covariate model. The deviance statistic is a relative measure to characterize the improvement of the covariate model (L_1) with respect to the stationary model (L_0). We do not attempt an intercomparison of the significance of the different indices here.

Roughly speaking, D indicates whether the covariate model is 'better' than the stationary model. The improvement is significant at the 1% level if $D > D_{99\%} = 6.634$, with the 99th percentile $D_{99\%}$ of the χ_k^2 distribution for k degrees of freedom, here $k = 1$.

The parameters are fitted with the R routine `gpd.fit` in the `ismev` package by maximum-likelihood estimation (MLE); see R Core Team (2013). This routine allows the inclusion of covariates and provides the log-likelihood results L_1 and L_0 for the covariate and stationary models; see (3).

A declustering of the extreme time series is not applied, since such methods may yield irreproducible results and inhibit the multivariate analysis of the two data sets. We fit the parameters of the GPD and compare the geographical distribution of their values, with emphasis on the two Northern Hemispheric storm tracks. We do not assess extremes of lows embedded in cyclone tracks, since the tracking of cyclones involves a further filter and introduces uncertainty and irreproducibility (Blender and Schubert, 2000; Raible *et al.*, 2008; Neu *et al.*, 2013).

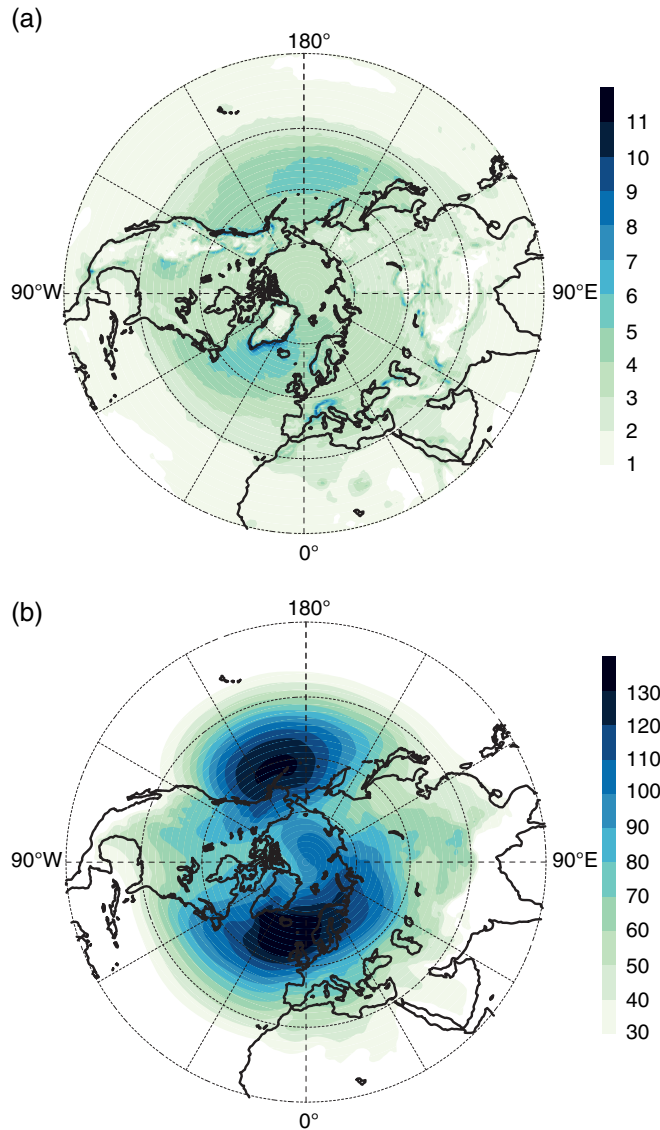


Figure 1. Standard deviation of (a) daily 850 hPa relative vorticity [10^{-5} s^{-1}] and (b) 1000 hPa GPH (m). [Colour figure can be viewed at wileyonlinelibrary.com].

4. Results

First we compare the standard deviations of vorticity and GPH to determine the regions of highest variability. A band-pass filter characterizing the midlatitude storm tracks is not applied. We then follow aims (i)–(iii) in section 1. The GPD parameters scale and shape yield information about the decay and possible upper bounds. The relationships of the large-scale flow and the GPD parameters are determined by extracting the covariate time series with the maximum significant deviance at each grid point. Finally, we determine the ratio of concurrent extremes, with special attention on avoiding misinterpretation due to artificial dependences.

4.1. Standard deviation

The standard deviation of the vorticity is concentrated in the storm tracks of the Northern Hemisphere (Figure 1). In both storm tracks, the maximum of the standard deviation of GPH is shifted eastward to the maximum in vorticity (the standard deviations are based on daily data). Note that the extremes of vorticity in the storm-track exit regions are not independent, since their return times are non-exponential (Blender *et al.*, 2015).

4.2. Extreme-value parameters

The scale parameters are highest in the midlatitude storm tracks (Figure 2). The scale parameter represents the spread and

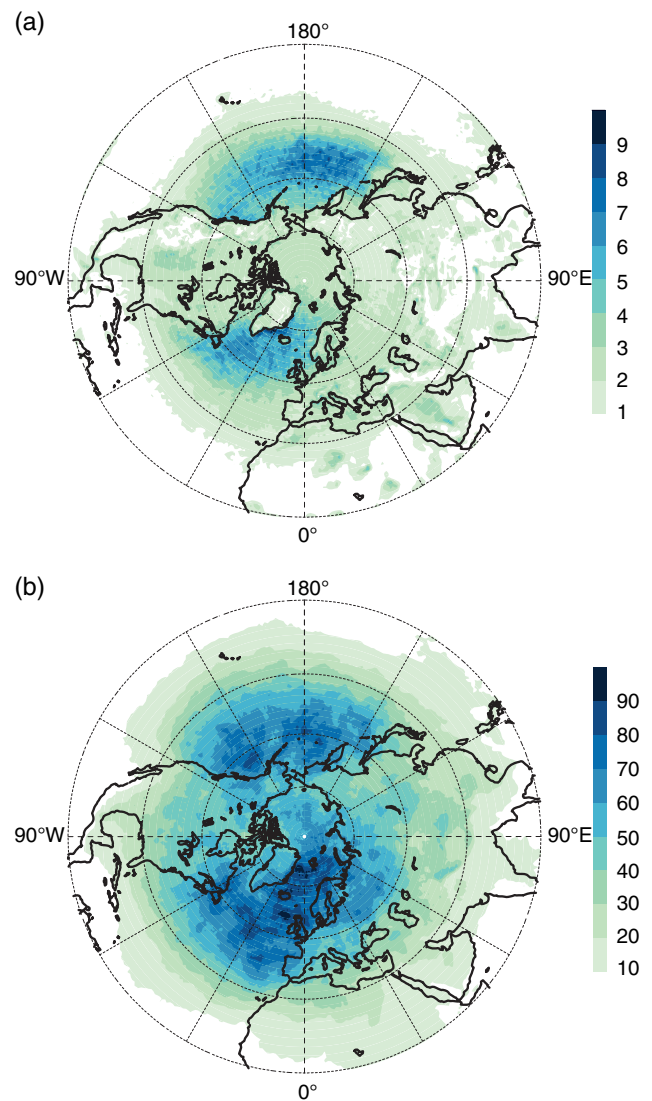


Figure 2. Scale parameter for (a) 850 hPa relative vorticity [10^{-5} s^{-1}] and (b) 1000 hPa GPH (m). [Colour figure can be viewed at wileyonlinelibrary.com].

determines the scaling of the exceedances $z = (x - u)/\sigma$ above threshold u in (1); for a vanishing shape parameter, the scale equals the exponential decay scale. In the Northern Hemispheric storm tracks, the scale parameters of vorticity and GPH behave differently. In the Pacific, the scale for vorticity decreases along the axes, while the scale of GPH shows two separated maxima. In the Atlantic, the scale increases along the axis for vorticity and GPH. The scale parameter follows the standard deviation (Figure 1) and the bipolar maximum of the scale in the North Pacific is consistent with the broad standard deviation.

The shape parameter for vorticity (Figure 3) is positive in the subtropics and decreases northward, with a zero crossing along 50°N in the North Atlantic and along 40°N in the North Pacific; along these lines the extremes are exponentially distributed (1). In the exit regions and on land, the shape parameter is mostly negative, which indicates either an upper physical bound or the lack of extreme data in support of the distribution. For GPH, the shape parameter is weakly negative except in a restricted region in the tropical Pacific. GPH extremes are obviously limited by upper bounds. This finding is explained by the averaging property of the inverse Laplacian for balanced flow.

4.3. Covariate models

Here, we assess the dependence of extreme value parameters on the large-scale flow through covariate modelling (section 3). For covariates, we consider the indices of the monthly mean large-scale flow anomalies NAO, PNA and Nino3.4. Our main

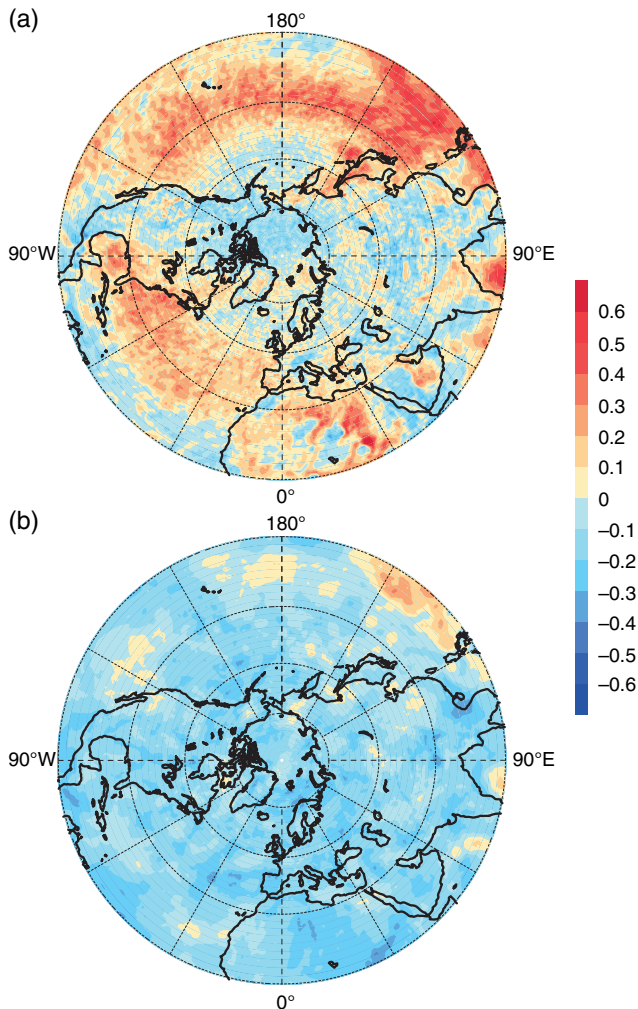


Figure 3. Shape parameter for (a) 850 hPa relative vorticity and (b) 1000 hPa GPH extremes. [Colour figure can be viewed at wileyonlinelibrary.com].

aim is to determine the statistical significance of a covariate model (2) relative to the stationary model, using the deviance statistic D defined in (3). The analysis is performed at every grid point for vorticity and GPH to determine the deviance for the scale and shape parameters. The best covariate model is selected by the maximum D . Furthermore, it has to achieve statistical significance, which is given if $D > D_{1-\alpha}$, where $D_{1-\alpha}$ is the $(1 - \alpha)$ quantile of the χ^2_1 distribution and α is the significance level; here, $\alpha = 1\%$ (Coles, 2001). The best models are displayed for the scale and shape parameters for vorticity (Figure 4) and GPH (Figure 5).

The best model pattern for vorticity (Figure 4) has a detailed structure indicating that the significance is a sample dependent random variable with a deviance statistic close to significance. We compared the analysis with the lower threshold $D_{95\%} = 3.841$ for the deviance corresponding to 5% significance and found similar results. A noteworthy outcome is that indices like NAO and PNA do not contribute significantly in the core regions of the North Atlantic and North Pacific storm tracks, as illustrated by the maxima in the daily standard deviation (Figure 1). The NAO and PNA phases have a significant impact on extremes, which does not correspond to a simple shift as is the case for the mean storm-track response to the teleconnection patterns. This might suggest a nonlinear response of the extremes to the teleconnection patterns. The NAO index is relevant in the northern and eastern subtropical North Atlantic. In the central tropical Pacific, the Nino3.4 index and PNA index show some coherent structure for scale and shape parameters (note that both are correlated with $r \approx 0.4$). The shape parameter follows the scale parameter, but is less predictable.

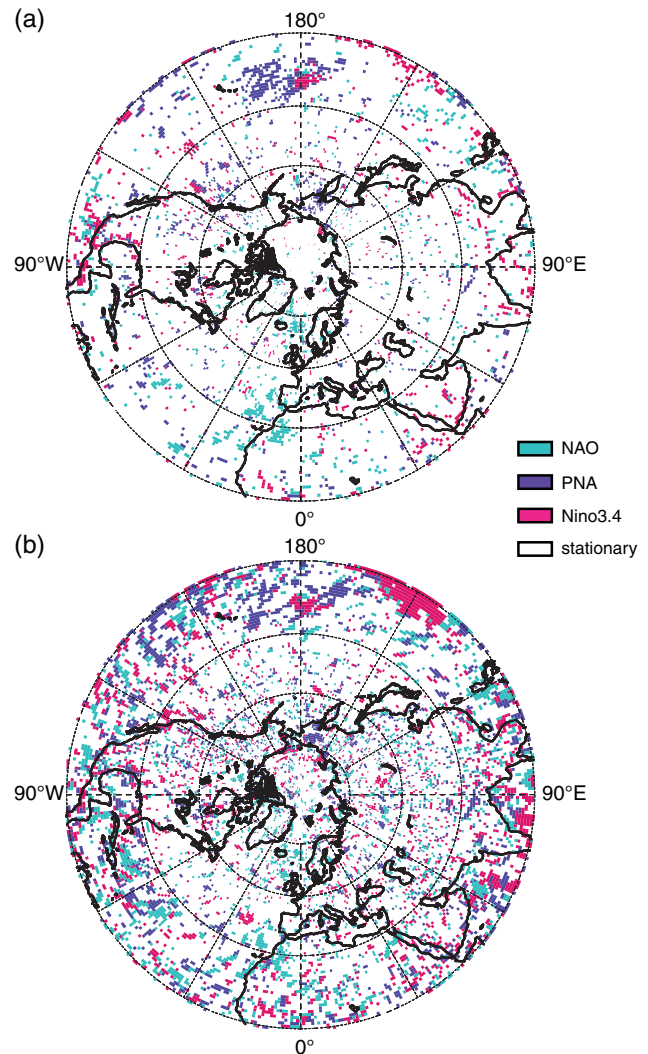


Figure 4. Vorticity extremes: best covariate model for (a) scale and (b) shape parameters. 1: stationary, 2: Nino3.4, 3: PNA, 4: NAO. [Colour figure can be viewed at wileyonlinelibrary.com].

The best models for the GPH parameters show more coherent patches than those for vorticity (Figure 5), most probably due to the coarse-grained character of this field. The NAO index dominates in the North Atlantic (the exit region of the storm track) and in the southern North Atlantic in both parameters. In the Pacific, unforeseen results are detected. While the indices for Nino3.4 and PNA are found for the scale parameter in the eastern Pacific, the steering of the shape parameter is less clear. The relationship between the frequency of deep cyclones and the PNA found by Gulev *et al.* (2001) is recovered in both parameters in the eastern North Pacific. The NAO steering in North America, however, is not found here. The most noteworthy finding is the presence of the NAO covariate in large parts of the Pacific, including Southeast Asia. Even in the central tropical Pacific, the NAO index is the best covariate for both parameters. This is also observed with the lower significance threshold $D_{95\%} = 3.841$. A similar dominant link between an index of the tropical cyclone activity and the NAO was found by Elsner and Kocher (2000), without a link to ENSO. A physical mechanism is given by the wave train described by Li *et al.* (2008) between Eurasia and southwestern China.

4.4. Dependence of extremes

A straightforward measure for the conditional probability for extremes of vorticity ζ and GPH, denoted as Z , is given by

$$P_{\zeta,Z}(p) = P(\zeta > \zeta_p | Z < Z_p) = \frac{P(\zeta > \zeta_p, Z < Z_p)}{P(Z < Z_p)}, \quad (4)$$

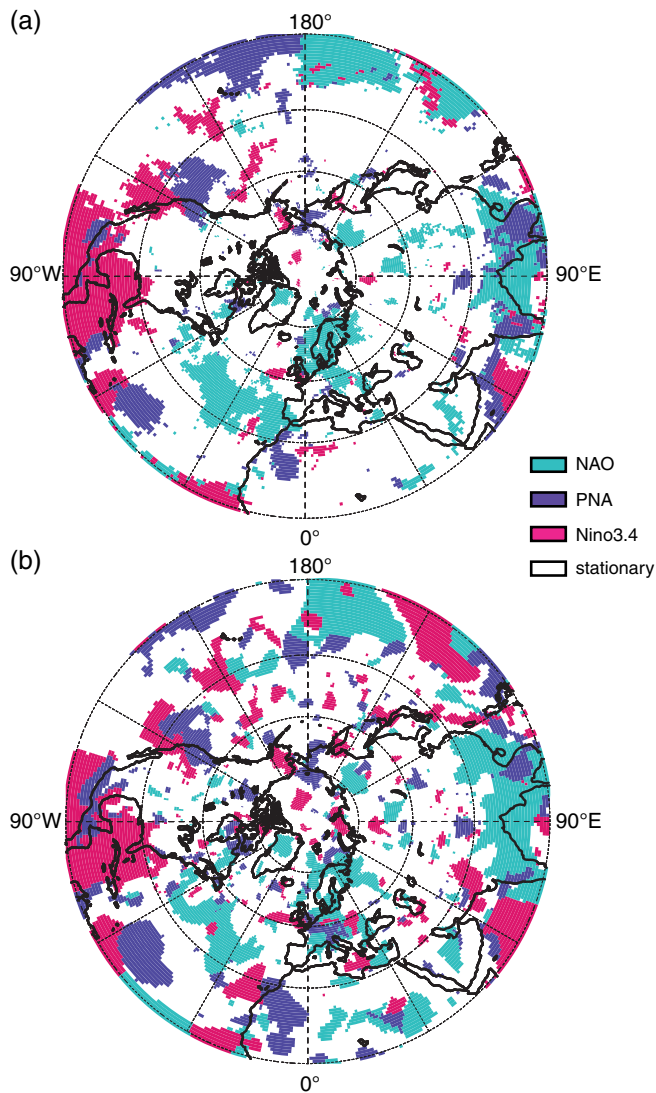


Figure 5. GPH extremes: best covariate model for (a) scale and (b) shape parameters. 1: stationary, 2: Nino3.4, 3: PNA, 4: NAO. [Colour figure can be viewed at wileyonlinelibrary.com].

where $P(\zeta > Z_p, Z < Z_p)$ is estimated by the number of coincidences of threshold crossings, $\zeta > \zeta_p$, with the threshold ζ_p and for Z below Z_p (Coles *et al.*, 1999). Since the extremes are defined by the same threshold $p = 0.9$, the probabilities for ζ and Z are the same, $P(\zeta > \zeta_p) = P(Z < Z_p) = 1 - p$. Therefore, the conditional probabilities are symmetric:

$$P_{\zeta,Z}(p) = P(\zeta > \zeta_p | Z < Z_p) = P(Z < Z_p | \zeta > \zeta_p). \quad (5)$$

The result for the conditional probability $P(\zeta > \zeta_p | Z < Z_p)$ in Figure 6 demonstrates relationships with values between 0.3 and 0.4 for relative vorticity and GPH in regions with balanced flow; there is no relationship in the Tropics and in higher latitudes.

Note that, in the measure $P_{\zeta,Z}(p)$ defined in (4), the quantile is constant with $p = 0.9$ for all grid points. This pertains to a common and standard perception of extremes. From a mathematical perspective, the extremal limit needs to be justified. Unfortunately, such a detailed analysis is difficult for large arrays of grid-point data.

Coles *et al.* (1999) consider the possible misinterpretation of the dependence of two variables X and Y . For identically distributed variables X and Y , they define the limit

$$\chi = \lim_{z \rightarrow z^*} P(X > z | Y > z), \quad (6)$$

where $z = z^*$ is given by support of the common marginal distribution, χ is within 0 and 1. Misinterpretation can appear

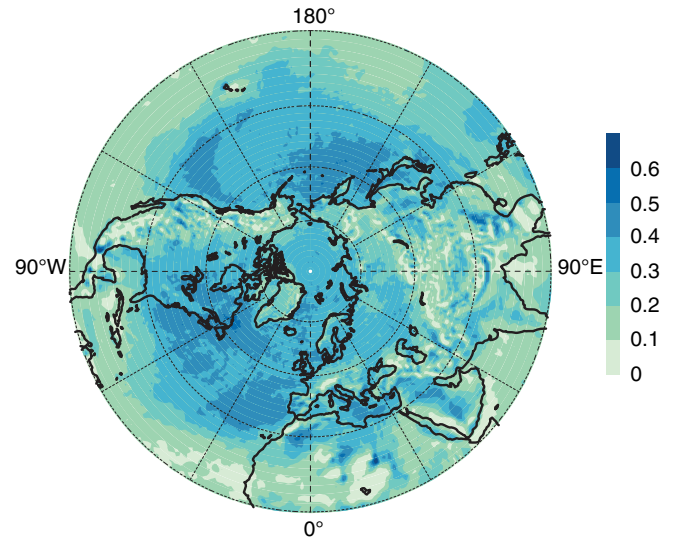


Figure 6. Estimated conditional probability for coinciding extremes of 850 hPa relative vorticity and 1000 hPa GPH. [Colour figure can be viewed at wileyonlinelibrary.com].

in the class of asymptotic independent data where $\chi = 0$. In real data, artificial values $\chi > 0$ can be detected below the limit z^* . To handle this case, Coles *et al.* (1999) defined an additional measure

$$\bar{\chi} = \lim_{u \rightarrow 1} \frac{\log P(X > u)}{\log P(X > u, Y > u)} - 1. \quad (7)$$

$\bar{\chi}$ is in the range $-1, \dots, 1$. The pair $(\chi, \bar{\chi})$ is suggested as a reliable measure for extreme dependence. The following limiting cases are used to define asymptotic dependence:

$$\chi > 0, \quad \bar{\chi} = 1, \quad (8)$$

where in this case the value of χ determines the dependence, whereas asymptotic independence is defined by

$$\chi = 0, \quad \bar{\chi} < 1, \quad (9)$$

where in this case the value of $\bar{\chi}$ determines the dependence.

In the analysis of $P_{\zeta,Z}(p)$ in (4), we obtained considerable degrees of dependence between extremes of ζ and Z (Figure 6). To exclude the aforementioned artificial dependences, we follow the approach suggested by Coles *et al.* (1999) and determine χ (6) and $\bar{\chi}$ (7). Due to the automatic calculation of the limits in the gridded data, this analysis is a rough estimation of χ and $\bar{\chi}$. Nevertheless, we assume that this additional aspect is helpful to exclude artificial dependence.

The measure χ in Figure 7 follows the conditional probability $P_{\zeta,Z}(p)$ to a large extent. The same property is visible in $\bar{\chi}$ in Figure 8. In areas where $\bar{\chi} \approx 1$, we may consider the value of χ as the dependence according to (8). This prevents the misinterpretation of $\chi > 0$. In areas where $\chi = 0$, we consider the value of $\bar{\chi}$ as a dependence measure according to (9). Thus we conclude that the relationship in $P(\zeta > \zeta_p | Z < Z_p)$ in Figure 6 is reliable and not an artefact with a hidden underlying independence of both variables in the storm tracks.

5. Summary and conclusions

In this study, the properties and dependences of extreme relative vorticity (at 850 hPa) and geopotential height (GPH at 1000 hPa) are determined in high-resolution ERA-Interim data (0.75°). The analysis covers the boreal winter seasons DJF during 1980–2014. Extreme behaviour is analyzed by POT independently for all grid points with a common 90th percentile threshold.

Three major aims underlie this study:

- (i) the POT analysis and the calculation of the scale and shape GPD parameters;

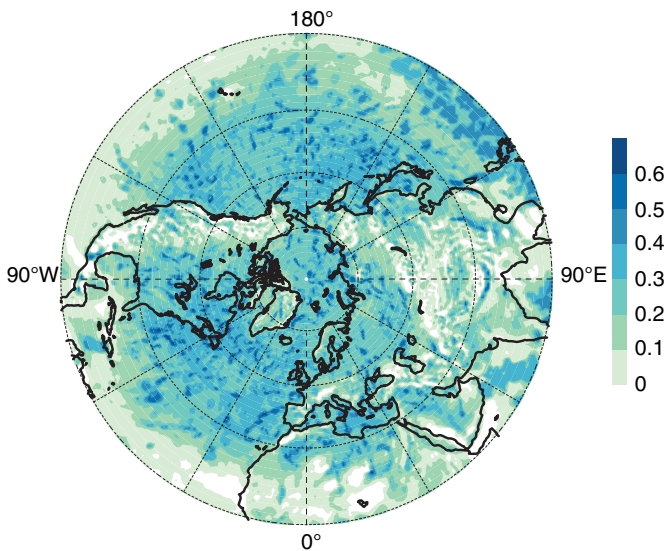


Figure 7. Dependence measure χ between 850 hPa relative vorticity and 1000 hPa GPH extremes. [Colour figure can be viewed at wileyonlinelibrary.com].

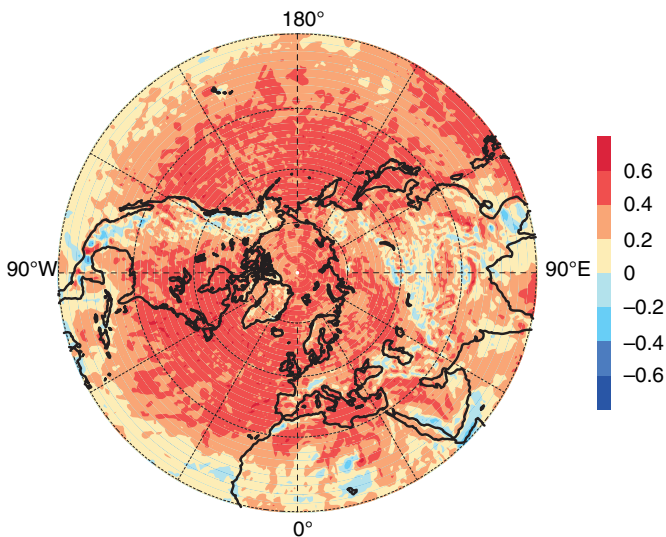


Figure 8. Dependence measure $\bar{\chi}$ between 850 hPa relative vorticity and 1000 hPa GPH extremes. [Colour figure can be viewed at wileyonlinelibrary.com].

- (ii) the significance of the large-scale covariates NAO, PNA and Nino3.4 as linear predictors for the GPD parameters; and
- (iii) the mutual dependence of the vorticity and GPH extremes in terms of a conditional probability.

We fit the two parameters of the GPD, scale and shape, by maximum-likelihood estimation. The behaviour of the scale parameter differs for vorticity and GPH. For vorticity, the scale parameter decreases along the storm-track axes in the North Atlantic and North Pacific. For GPH, the scale parameter shows no decay but a broad distribution. In the North Pacific, the scale parameter indicates a bipolar distribution, with a split into western and eastern parts.

The shape parameters for vorticity decrease along the storm-track axes and change sign, indicating upper bounds in the exit regions. In the North Atlantic, the boundary with zero shape is roughly along 50°N and in the North Pacific along 40°N, where the probability density is exponentially distributed. The shape parameters are weakly negative for vorticity on land, while the GPH shape parameters for GPH are weakly negative globally.

Covariate models for the two parameters using monthly mean indices for NAO, PNA and Nino3.4 are assessed and compared with the stationary model. Clearly, there is an overlap of the information in PNA and Nino3.4, which is not assessed here.

The global structure is remarkably diverse, with a dominance of the stationary model, in particular for the shape parameters and for vorticity in general. Only in a few cases are the covariates interpretable predictors: for example, the Nino3.4 index explains the two parameters of vorticity in the tropical Pacific and the NAO the GPH scale in northern and Central Europe and in the northern tropical Atlantic. A surprising finding is the clear dominance of the NAO covariate in the central tropical Pacific and southeast Asia. This finding corroborates previous analyses of Li *et al.* (2008), detecting a Eurasian wave-train, and Elsner and Kocher (2000), who found a linear relationship between the NAO and global tropical cyclone counts.

The relationship between GPH extremes and large-scale teleconnection patterns is significant in a few regions. This can be considered as a basis for the modelling of extremes (Coles, 2001). The relationship is much weaker for vorticity extremes, most probably because the teleconnections are pressure-based.

The mutual dependence of vorticity and GPH extremes is highest in the midlatitude ocean basins, with conditional probabilities in the range 0.3–0.5. This includes the two Northern Hemispheric storm tracks. In mountainous regions and in the Tropics, the conditional probability is negligible. To avoid a misinterpretation of this result, the analysis of Coles *et al.* (1999) is applied, with two measures that concurrently determine extremal dependence and exclude artificial dependence in real data of independent processes.

The frequency of the concurrent extremes in vorticity and GPH can be crucial for use of the fields as indicators of severe storms. Although the fields are related, due to the geostrophic balance, there is no dynamic relationship between the extremes at the grid points.

The absence of a coincidence in high orography is expected, because both fields (mainly 1000 hPa GPH) are interpolated. This is accounted for in most cyclone-tracking algorithms by the exclusion of regions with an orography of 1000 or 1500 m. The analyses have been repeated for the coarser resolutions of 1.5 and 2.5° in the ERA-Interim data. The main results for the covariate models and the dependence are confirmed. The present study might have relevance for the detection and tracking of extreme cyclones and their interpretation.

Acknowledgement

We are grateful for many discussions with the members of the Intercomparison of MidLatitude Storm Diagnostics (IMILAST) project (contact: Urs Neu, Bern). CR is grateful for the support provided by the Mobilab lab for climate risk and natural hazards (Mobilab) and the Swiss National Science foundation (grant no.200020 147174). This study has been supported by the German Research Foundation through the cluster of excellence CliSAP (EXC177) at the University of Hamburg.

References

- Blender R, Schubert M. 2000. Cyclone tracking in different spatial and temporal resolutions. *Mon. Weather Rev.* **128**: 377–384.
- Blender R, Fraedrich K, Lunkeit F. 1997. Identification of cyclone-track regimes in the North Atlantic. *Q. J. R. Meteorol. Soc.* **123**: 727–741, doi: 10.1002/qj.49712353910.
- Blender R, Raible CC, Lunkeit F. 2015. Non-exponential return time distributions for vorticity extremes explained by fractional Poisson processes. *Q. J. R. Meteorol. Soc.* **141**: 249–257, doi: 10.1002/qj.2354.
- Coles S. 2001. *An Introduction to Statistical Modeling of Extreme Values*, Vol. 208. London: Springer.
- Coles S, Heffernan J, Tawn J. 1999. Dependence measures for extreme value analyses. *Extremes* **2**: 339–365, doi: 10.1023/A:1009963131610.
- Dee DP, Uppala SM, Simmons AJ, Berrisford P, Poli P, Kobayashi S, Andrae U, Balmaseda MA, Balsamo G, Bauer P, Bechtold P, Beljaars ACM, van de Berg L, Bidlot J, Bormann N, Delsol C, Dragani R, Fuentes M, Geer AJ, Haimberger L, Healy SB, Hersbach H, Hólm EV, Isaksen L, Kållberg P, Köhler M, Matricardi M, McNally AP, Monge-Sanz BM, Morcrette JJ, Park BK, Peubey C, de Rosnay P, Tavolato C, Thépaut JN, Vitart F. 2011. The ERA-Interim reanalysis: Configuration and performance

- of the data assimilation system. *Q. J. R. Meteorol. Soc.* **137**: 553–597, doi: 10.1002/qj.828.
- Elsner JB, Kocher B. 2000. Global tropical cyclone activity: A link to the North Atlantic Oscillation. *Geophys. Res. Lett.* **27**: 129–132, doi: 10.1029/1999GL010893.
- Flocas HA, Simmonds I, Kouroutzoglou J, Keay K, Hatzaki M, Bricolas V, Asimakopoulos D. 2010. On cyclonic tracks over the eastern Mediterranean. *J. Clim.* **23**: 5243–5257, doi: 10.1175/2010JCLI3426.1.
- Franzke CLE. 2013. Persistent regimes and extreme events of the North Atlantic atmospheric circulation. *Philos. Trans. R. Soc. London, Ser. A* **371**: 20120518, doi: 10.1098/rsta.2011.0471.
- Franzke C, Woollings T, Martius O. 2011. Persistent circulation regimes and preferred regime transitions in the North Atlantic. *J. Atmos. Sci.* **68**: 2809–2825.
- Gulev KS, Zolina O, Grigoriev S. 2001. Extratropical cyclone variability in the Northern Hemisphere winter from the NCEP/NCAR reanalysis data. *Clim. Dyn.* **17**: 795–809, doi: 10.1007/s003820000145.
- Held H, Gerstengarbe FW, Pardowitz T, Pinto JG, Ulbrich U, Born K, Donat MG, Karremann MK, Leckebusch GC, Ludwig P, Nissen KM, Österle H, Prahlf BF, Werner PC, Befort DJ, Burghoff O. 2013. Projections of global warming-induced impacts on winter storm losses in the German private household sector. *Clim. Change* **121**: 195–207.
- Hodges KI. 1994. A general method for tracking analysis and its application to meteorological data. *Mon. Weather Rev.* **122**: 2573–2586.
- Klawe M, Ulbrich U. 2003. A model for the estimation of storm losses and the identification of severe winter storms in Germany. *Nat. Hazards Earth Syst. Sci.* **3**: 725–732.
- Koenig W, Sausen R, Sielmann F. 1993. Objective identification of cyclones in GCM simulations. *J. Clim.* **6**: 2217–2231.
- Leckebusch GC, Ulbrich U. 2004. On the relationship between cyclones and extreme windstorm events over Europe under climate change. *Global Planet. Change* **44**: 181–193, doi: 10.1016/j.gloplacha.2004.06.011.
- Li J, Yu R, Zhou T. 2008. Teleconnection between NAO and climate downstream of the Tibetan plateau. *J. Clim.* **21**: 4680–4690, doi: 10.1175/2008JCLI2053.1.
- Lucarini V, Faranda D, Wouters J, Kuna T. 2014. Towards a general theory of extremes for observables of chaotic dynamical systems. *J. Stat. Phys.* **154**: 723–750, doi: 10.1007/s10955-013-0914-6.
- Majda A, Franzke CLE, Crommelin D. 2009. Normal forms for reduced stochastic climate models. *Proc. Natl. Acad. Sci. U.S.A.* **106**: 3649–3653, doi: 10.1073/pnas.0900173106.
- Malmquist D. 1999. 'European windstorms and the North Atlantic Oscillation: Impacts, characteristics, and predictability', Risk Prediction Initiative, Bermuda Biological Station for Research, Inc. Bermuda, Technical report 2. RPI Series.
- MunichRe. 2010. 'Significant winterstorms Europe 1980–2009. Overall losses'. Technical report 60, Munich. www.munichre.com (accessed 12 November 2016).
- MunichRe. 2015. 'Loss events worldwide 1980–2014', Technical report 20. Munich. www.munichre.com (accessed 12 November 2016).
- Murray RJ, Simmonds I. 1991a. A numerical scheme for tracking cyclone centers from digital data. Part II: Application to January and July general circulation model simulations. *Aust. Meteorol. Mag.* **39**: 167–180.
- Murray RJ, Simmonds I. 1991b. A numerical scheme for tracking cyclone centres from digital data. Part I: Development and operation of the scheme. *Aust. Meteorol. Mag.* **39**: 155–166.
- Neu U, Akperov MG, Bellenbaum N, Benestad R, Blender R, Caballero R, Cocozza A, Dacre HF, Feng Y, Fraedrich K, Grieger J, Gulev S, Hanley J, Hewson T, Inatsu M, Keay K, Kew SF, Kindem I, Leckebusch GC, Liberato MLR, Lionello P, Mokhov II, Pinto JG, Raible CC, Reale M, Rudeva I, Schuster M, Simmonds I, Sinclair M, Sprenger M, Tilinina ND, Trigo IF, Ulbrich S, Ulbrich U, Wang XL, Wernli H. 2013. Imilast: A community effort to intercompare extratropical cyclone detection and tracking algorithms. *Bull. Am. Meteorol. Soc.* **94**: 529–547, doi: 10.1175/BAMS-D-11-00154.1.
- Pinto JG, Zacharias S, Fink AH, Leckebusch GC, Ulbrich U. 2008. Factors contributing to the development of extreme North Atlantic cyclones and their relationship with the NAO. *Clim. Dyn.* **32**: 711–737, doi: 10.1007/s00382-008-0396-4.
- Raible CC. 2007. On the relation between extremes of midlatitude cyclones and the atmospheric circulation using ERA40. *Geophys. Res. Lett.* **34**: L07703, doi: 10.1029/2006GL029084.
- Raible CC, Della-Marta P, Schwierz C, Wernli H, Blender R. 2008. Northern Hemisphere extratropical cyclones: A comparison of detection and tracking methods and different reanalyses. *Mon. Weather Rev.* **136**: 880–897, doi: 10.1175/2007MWR2143.1.
- R Core Team. 2013. The R Project for Statistical Computing, Technical report. Vienna. <http://www.R-project.org> (accessed 12 November 2016).
- Schwierz C, Köllner-Heck P, Mutter EZ, Bresch DN, Vidale PL, Wild M, Schär C. 2010. Modelling European winter wind storm losses in current and future climate. *Clim. Change* **101**: 485–514.
- Siens F, Schneidereit A, Blender R, Fraedrich K, Lunkeit F. 2010. Extreme value statistics for North Atlantic cyclones. *Tellus A* **62**: 347–360, doi: 10.1111/j.2010.00449.x.
- Simmonds I, Keay K. 2000. Mean southern hemisphere extratropical cyclone behaviour in the 40-year NCEP-NCAR reanalysis. *J. Clim.* **13**: 873–885.
- Towler E, Rajagopalan B, Gilleland E, Summers RS, Yates D, Katz RW. 2010. Modeling hydrologic and water quality extremes in a changing climate: A statistical approach based on extreme value theory. *Water Resour. Res.* **46**: W11504, doi: 10.1029/2009WR008876.
- Ulbrich U, Leckebusch GC, Grieger J, Schuster M, Akperov M, Bardin MY, Feng Y, Gulev S, Inatsu M, Keay K, Kew SF, Liberato MLR, Lionello P, Mokhov II, Neu U, Pinto JG, Raible CC, Reale M, Rudeva I, Simmonds I, Tilinina ND, Trigo IF, Ulbrich S, Wang XL, Wernli H. 2013. Are greenhouse gas signals of northern hemisphere winter extra-tropical cyclone activity dependent on the identification and tracking algorithm? *Meteorol. Z.* **22**: 61–68, doi: 10.1127/0941-2948/2013/0420.
- Welker C, Martius O. 2014. Decadal-scale variability in hazardous winds in Northern Switzerland since end of the 19th century. *Atmos. Sci. Lett.* **15**: 86–91, doi: 10.1002/asl2.467.